Quaternary uplift astride the aseismic Cocos Ridge, Pacific coast, Costa Rica

THOMAS W. GARDNER
DAVID VERDONCK
NICHOLAS M. PINTER*
RUDY SLINGERLAND
KEVIN P. FURLONG
Department of Geosciences, Pennsylvania State University, University Park, Pennsylvania 16802

THOMAS F. BULLARD*
STEPHEN G. WELLS*
Department of Geology, University of New Mexico, Albuquerque, New Mexico 87131

ABSTRACT

The Pacific coast of Costa Rica lies within the Central American forearc and magmatic-arc region that was created by northeastward subduction of the Cocos plate beneath the Caribbean plate at the Middle America Trench. From the Península de Nicoya southeastward toward the Península de Osa and the Península de Burica on the Panamanian border, the Middle America Trench loses its physiographic expression where it intersects the aseismic Cocos Ridge. Interaction between subduction of the buoyant, aseismic Cocos Ridge and the overriding Caribbean plate is invoked to explain the variation in rates of vertical crustal uplift along a coastal transect from Nicoya to Burica. The Pliocene and Pleistocene stratigraphic record and Holocene marine terraces and beach ridge complexes indicate that maximum rates of crustal uplift have occurred on the Península de Osa, immediately landward of the aseismic Cocos Ridge. Crustal uplift rates decrease northwest toward the Península de Nicoya, and to a lesser extent southwest toward the Península de Burica.

The late Quaternary stratigraphy on the Península de Osa is subdivided into two major chronostratigraphic sequences from groupings of radiocarbon dates. Crustal uplift rates calculated from these sequences systematically decrease from 6.5 to 2.1 m/ka northeast across the peninsula. Deformation of the peninsula is modeled as uplifted and down-to-the-northeast–tilted fault blocks with an angular rotation rate of 0.03° to 0.06° per thousand years. Although less well constrained, crustal uplift rates on the Península de Nicoya, 200 km to the northwest of the Península de Osa, vary from <1 m/ka for Pliocene and Pleistocene sediments to 2.5 m/ka for Holocene marine terraces. In the Quepos region, 100 km to the northwest of the Península de Osa, calculated uplift rates derived from incision of late Quaternary fluvial terraces range from 0.5 to 3.0 m/ka. On the Península de Burica, only 60 km to the southwest of the Península de Osa, calculated uplift rates range from 4.7 m/ka for a late Holocene marine terrace to 1.2 m/ka for post–late Pliocene deep-sea sediments.

The variations in calculated uplift rates on the Península de Osa constrain a dynamic model for subduction of the Cocos Ridge and the resulting uplift of the overriding Caribbean plate. Deflection of the Caribbean plate is modeled using various effective elastic thicknesses as the response of an elastic plate to the buoyant force of the subducted Cocos Ridge. Because the shape of the subducted end of the Cocos Ridge is unknown, two scenarios are evaluated: (1) a radially symmetric ridge with a slope similar to the slope of the flanks of the ridge and (2) a ridge where the subducted end was truncated by the Panama fracture zone. The best-fit model utilizes a truncated ridge that has been subducted during the past 0.5 m.y. ~50 km beneath the overriding Caribbean plate, which has an effective elastic thickness of 5 km. The model predicts that the highest uplift rate should be ~3.7 m/ka and occur on the southwest coast of the Península de Osa. The rate of uplift slows considerably to the northeast and indicates that the Península de Osa is tilting to the northeast, which agrees with observations in that region. The predicted uplift rate attributed to aseismic ridge subduction also decreases along the coast both north and south of the Península de Osa, resulting in little uplift that can be attributed to Cocos Ridge subduction in the northwestern portions of the Península de Nicoya.

INTRODUCTION

The Pacific coast of Costa Rica is part of the Central American forearc and magmatic-arc region created by northeastward subduction of the Cocos plate beneath the Caribbean plate at the Middle America Trench. Subduction of oceanic lithosphere is often cited as the driving force for deformation in arc and forearc regions (Molnar and Atwater, 1978; Jordan and others, 1983). Although the deformational processes are known in general (Cross and Pilger, 1982; Stockmal, 1983; Wang and Shi, 1984), complications arise from subduction of anomalous bathymetric features in the form of oceanic plateaus, fracture-zone ridges, or in the case of southeastern Costa Rica (Fig. 1), an aseismic ridge. The more noticeable complications from subduction of anomalous bathymetric features include relative seismic quiescence or gaps (Vogt and others, 1976; Kelleher and McCann, 1976; Astiz and Kanamori, 1984; Montero, 1986; Adamek and others, 1987), volcanic-arc segmentation and/or quiescence (Stoiber and Carr, 1973; McGeary and others, 1985; Gardner and others, 1987), and rapid crustal uplift of the overriding plate (Chung and Kanamori, 1978; Alt and others, 1980; Taylor and others, 1980; Corrigan and Mann, 1986; Hsü and others, 1986; Heil and Silver, 1987; Pinter and others, 1987; Gardner and others, 1987; Bullard and others, 1988; Verdonck and Furlong, 1988; Wells and others, 1988).

Our goal is to better understand one specific case among these phenomena—the vertical motions of the overriding Caribbean plate in response to subduction of oceanic lithosphere

*Present addresses: (Pinter) Department of Geological Sciences, University of California, Santa Barbara, California 93106; (Bullard) Geomatrix Consultants, 100 Pine Street, 10th floor, San Francisco, California 94111; (Wells) Department of Earth Sciences, University of California, Riverside, California 92521.

Geological Society of America Bulletin, v. 104, p. 219–232, 14 figs., 2 tables, February 1992.

containing the aseismic Cocos Ridge. We first document this uplift by using the magnitudes, rates, and locations of vertical crustal deformation along the Pacific coast of Costa Rica obtained from uplifted Quaternary marine terraces, fluvial terraces, and marine sedimentary sequences. We then develop a dynamic model constrained by the observed Quaternary uplift.

The study area is located along the Pacific coast of Costa Rica (Fig. 1) where subduction of the aseismic Cocos Ridge is hypothesized to be causing uplift of the overriding Caribbean plate (Vogt and others, 1976; Gardner and others, 1987; Wells and others, 1988; Corrigan and others, 1990). The Pacific coast of Costa Rica provides an appropriate site for such a study for several reasons. First, normal subduction characterized by a well-defined Benioff zone (Fig. 2) is occurring along the northwest Pacific coast seaward of the Península de Nicoya (Matumoto and others, 1977; Lundberg, 1983; Burbach and others, 1984; Bourgois and others, 1984; Shipley and Moores, 1986) and active arc volcanism is occurring inland. Second, Cocos Ridge subduction is occurring seaward of the Península de Osa (van Andel and others, 1971; Vogt and others, 1976; Hey, 1977; Lonsdale and Klitgord, 1978; Okaya and Ben-Avraham, 1987). Shallow, diffuse, seismic activity beneath the Península de Osa indicates underthrusting (Adamek and others, 1987), but without a well-defined Benioff zone (Fig. 2). Thus, we can document the change in uplift rate with distance from the Cocos Ridge along a coastal transect from the northwest (Península de Nicoya) to the southeast (Península de Osa and Península de Burica, Fig. 1). Third, the late Neogene and Quaternary history of Cocos Ridge subduction (Fig. 3) is reasonably well constrained by reconstructed plate motions (van Andel and others, 1971; Hey, 1977; Lonsdale and Klitgord, 1978; Gardner and others, 1987). At approximately 8 Ma when the Panama fracture zone is hypothesized to have propagated through to the Middle America Trench, the Panama triple junction was located offshore of the Península de Nicoya in northwestern Costa Rica (Fig. 3). At that time, subduction in the vicinity of the Península de Osa in southwestern Costa Rica was oblique and slower. Subsequent, southeast migration of the Panama triple junction along the Middle America Trench at an approximate rate of 35 m/ka gradually re-established subduction between the Cocos and Caribbean plates. At about 1 Ma, the Cocos Ridge began to be subducted in the vicinity of the Península de Osa. It is the subduction of the Cocos Ridge that we hypothesize to be causing the observed uplift in the overriding Caribbean plate.

We first present the late Quaternary stratigraphy for the Península de Osa landward of the Cocos Ridge, from which we derive depths of deposition. We then calculate an uplift from the paleodepositional depths, radiocarbon ages, and a local sea-level curve and compare uplift rates among locations along the Middle America Trench from the Península de Nicoya to the Península de Burica. Finally, we develop a dynamic model that is constrained by the uplift rates on the Península de Osa. We use the elastic model of Moretti and Ngokwey (1985) wherein the overriding lithosphere is assumed to behave as a perfectly elastic plate that is deflected upward due to the buoyancy of the subducting ridge.

STRATIGRAPHY OF THE PENÍNSULA DE OSA

Stratigraphic Framework

The Península de Osa (Fig. 4) is 400 km^2 in area and consists of a narrow coastal piedmont surrounding a mountainous core that exceeds

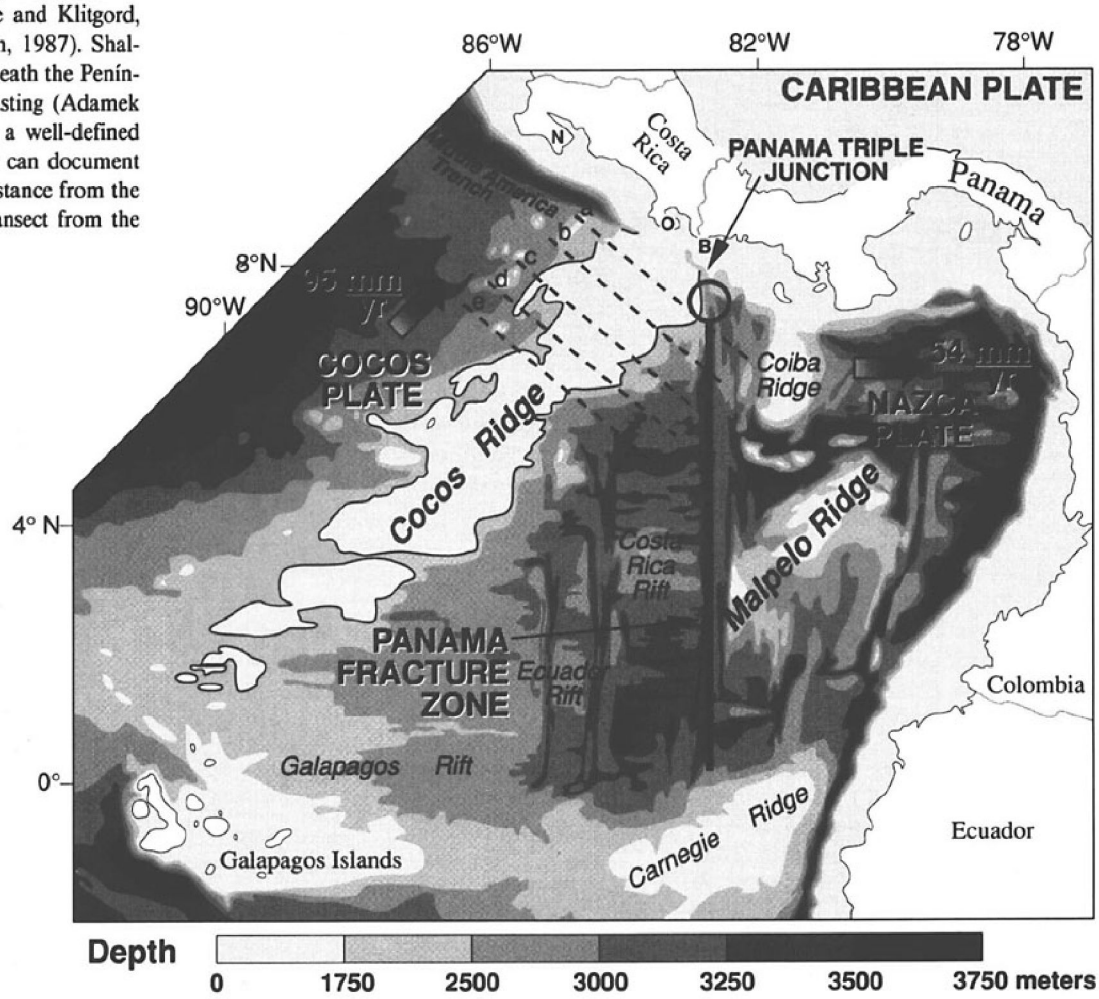

Figure 1. Location of the Cocos Ridge and major crustal features within the Panama Basin. Bathymetry contours from Lonsdale and Klitgord (1978). Modern plate motions for the eastern equatorial Pacific are based on the RM2 plate motion model of Minster and Jordan (1978). Cocos Ridge is outlined by the 1,750 m bathymetry contour. O, Península de Osa; B, Península de Burica; N, Península de Nicoya. Bathymetry cross sections a through e are shown in Figure 11.

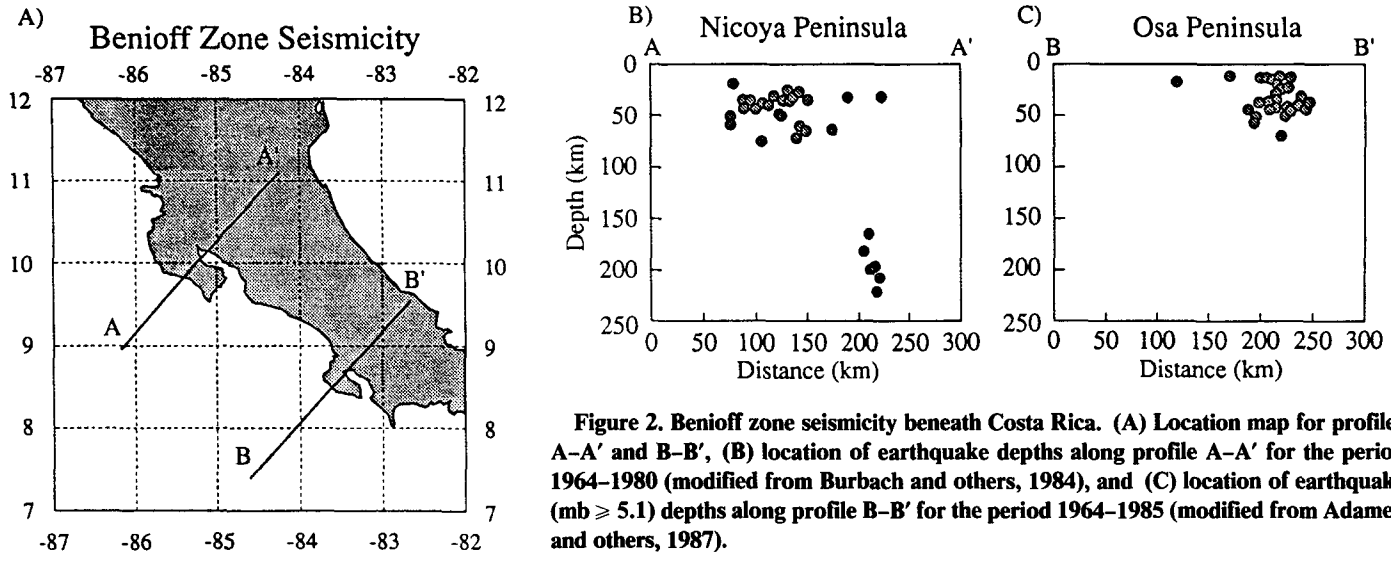

Figure 2. Benioff zone seismicity beneath Costa Rica. (A) Location map for profiles A–A′ and B–B′, (B) location of earthquake depths along profile A–A′ for the period 1964–1980 (modified from Burbach and others, 1984), and (C) location of earthquake (mb ≥ 5.1) depths along profile B–B′ for the period 1964–1985 (modified from Adamek and others, 1987).

700 m in elevation. The general stratigraphic framework of the peninsula is reasonably well known and consists of three units. The basement sequence, Nicoya Complex of Santonian to Lutetian age (Tournon, 1984), is composed of basaltic lavas, intrusive dolerites, and gabbros with interbedded pelagic limestones, argillites, and cherts (Barritt and Berrangé, 1987) that are exposed along incised valleys within the mountainous core of the peninsula and along the southern coast (Lew, 1983; Barritt and Berrangé, 1987). The basement is overlain unconformably by a Pliocene to Holocene sequence of shallowing-upward, locally derived, conglomerates, sandstones, siltstones, and claystones (Lew, 1983; Barrett and Berrangé, 1987) that record the progressive uplift of the peninsula. This sequence has been formally subdivided into the Charco Azul and Armuelles Formations (Manual de Geología de Costa Rica, 1984). It is the late Quaternary (post–40 ka) shallow-marine, beach ridge, and estuarine portion of this record that is the focus of this study.

Late Quaternary Stratigraphy

Late Quaternary deposits crop out extensively in stream banks in the foothills, piedmont, and coastal plain along the eastern portion of the peninsula (Fig. 4). Fifteen stratigraphic sections (Figs. 5 and 6) illustrate the geometries, facies associations, and radiocarbon ages of the late Quaternary stratigraphy on the Península de Osa. The strata are subdivided into two chronostratigraphic sequences (Fig. 7), using radiometric ages (Table 1, column 3). Chronostratigraphic sequence I consists of middle to late Holocene (0 to 7150 yr B.P.) relatively unconsolidated, sub-horizontal sands and gravels. Chronostratigraphic sequence II consists of late Pleistocene (20,140 to greater than 36,000 yr B.P.) semi-lithified, jointed and tilted, interstratified, mudstones and silty sandstones, pebbly mudstones, and conglomerates. Chronostratigraphic sequence II can be divided into three subunits, A, B, and C, on the basis of clusterings of radiocarbon ages between 20,140 and 26,770 yr B.P., between 29,780 and 35,290 yr B.P., and older than 36,000 yr B.P., respectively. Two of these age groups correspond to global glacio-eustatic phases: falling sea level to the late Pleistocene minimum (subunit A), and rising sea level between the late Pleistocene local min-

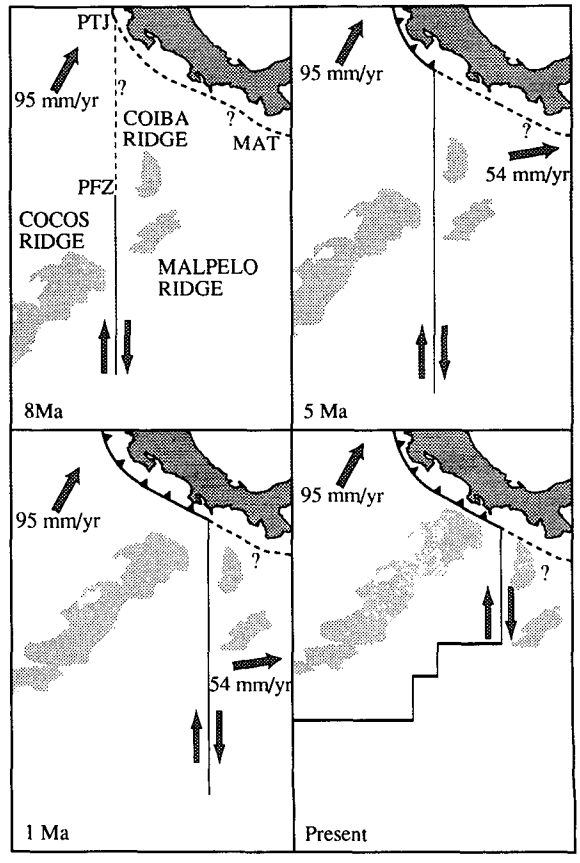

Figure 3. Plate tectonics of the eastern equatorial Pacific at 8 Ma, 5 Ma, 1 Ma, and Present, showing the movements of the Panama triple junction (PTJ), Cocos Ridge, and Panama fracture zone (PFZ). Also shown are the Middle America Trench (MAT) and the Coiba and Malpelo Ridges, which are believed to have been connected to the Cocos Ridge (modified after Gardner and others, 1987).

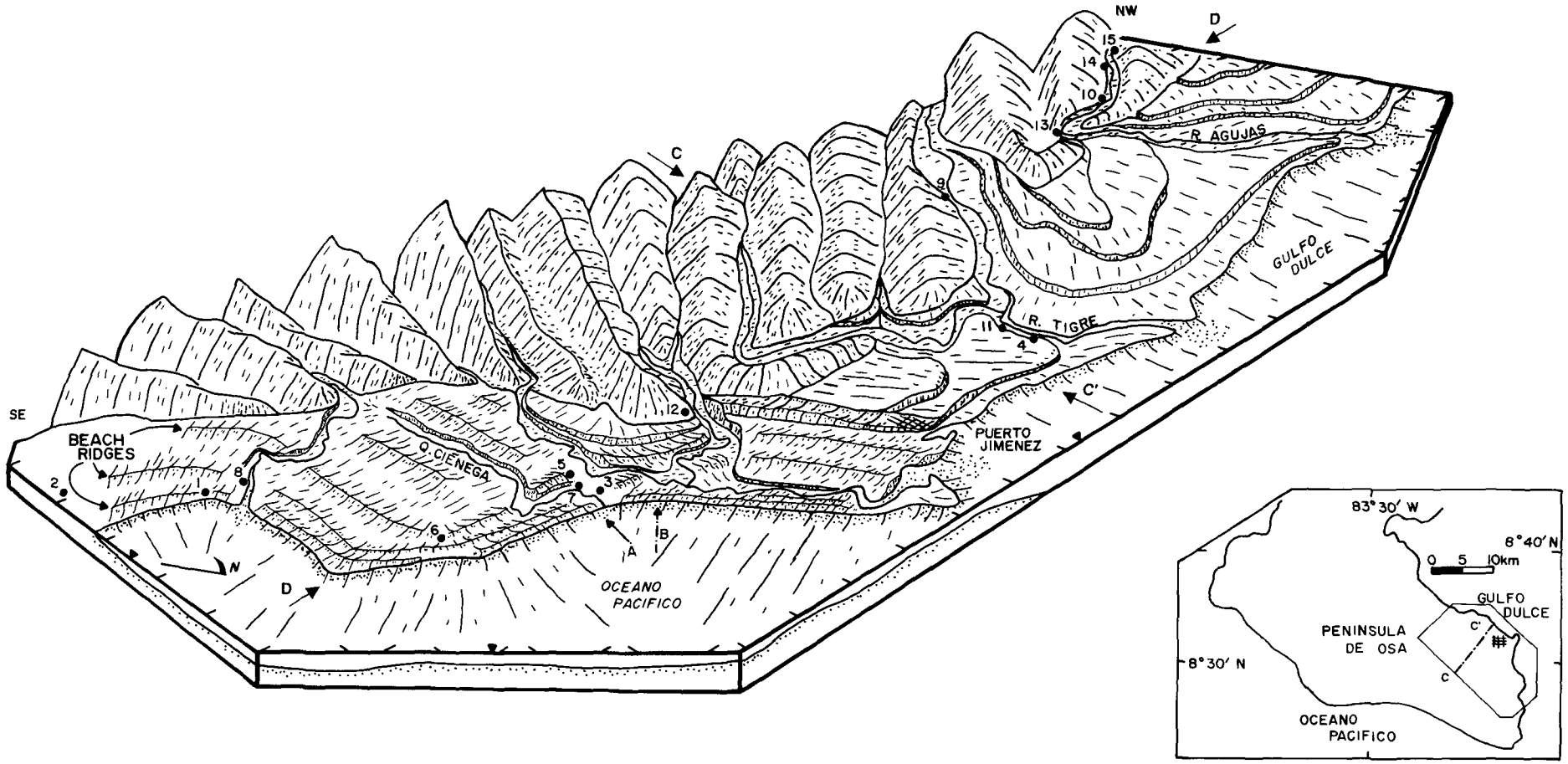

Figure 4. Eastern portion of the Península de Osa as viewed from a two-point perspective block diagram, looking toward the west. Tick marks along edge of block are in kilometers. Numbered solid dots denote sample sites (Table 1) and corresponding stratigraphic columns in Figure 5. Line A gives location of surveyed, topographic profile in Figure 5a. Line B gives general location of Figure 7. Line C–C′ (inset and block diagram) gives location of x axis for uplift rates in Figure 9. Line D gives approximate location and orientation of fault zone in Figure 9. Solid triangle indicates mean sea level.

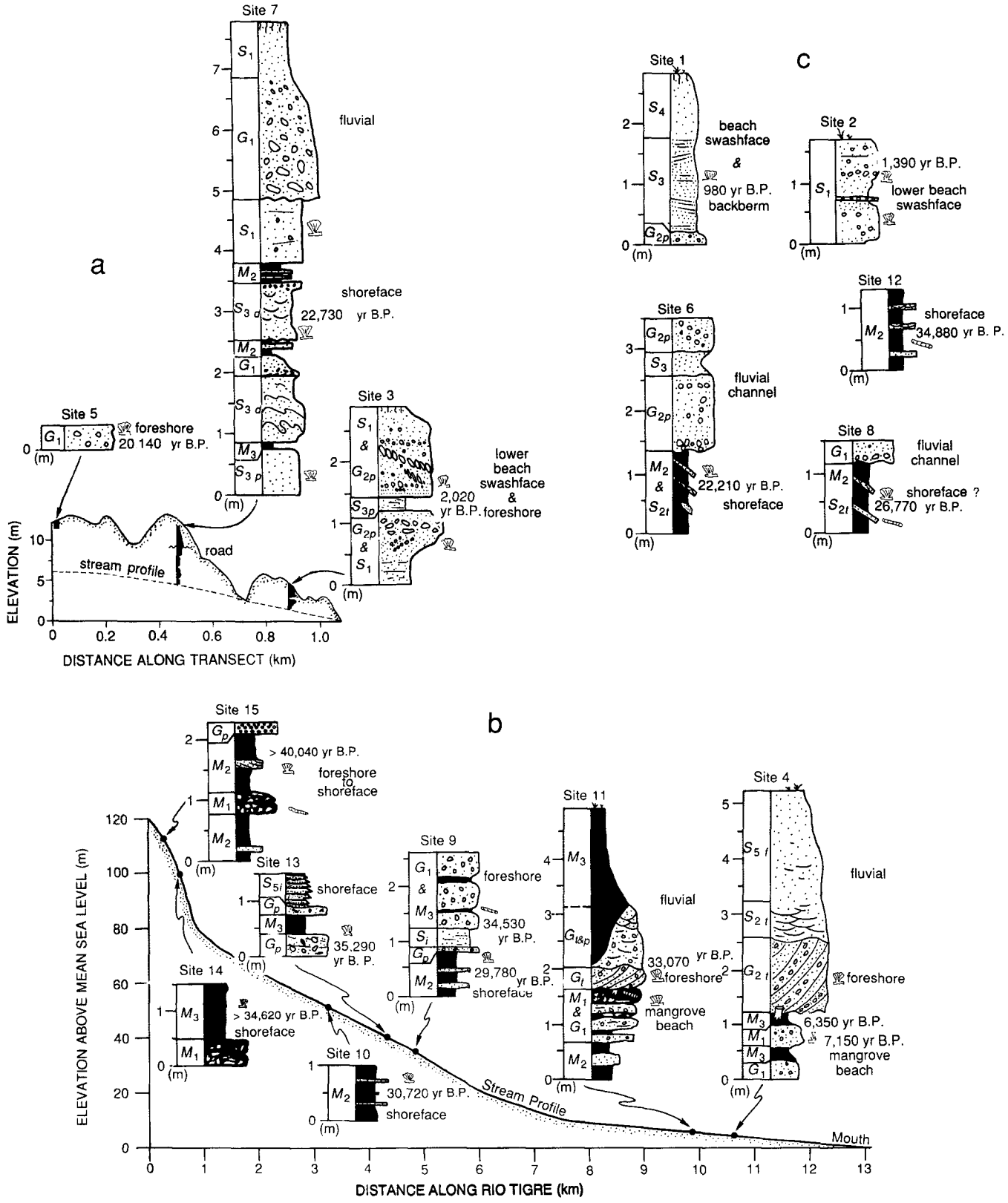

Figure 5. (a) Topographic cross section and related stratigraphic columns for line A (Fig. 4), illustrating the beach ridge morphology and longitudinal stream profile along Quebrada Ciénega. See Figure 6 for facies descriptions. (b) Longitudinal profile along the Rio Tigre (Fig. 4) and related stratigraphic columns. Sites 10, 13, 14, and 15 are projected along strike from the Rio Agujas to the Rio Tigre. (c) Stratigraphic columns for isolated outcrops along the eastern portion of the Península de Osa (Fig. 4). Sites 1 and 2, part of the late Holocene beach ridge sequence that constitutes chronostratigraphic sequence I, can be traced laterally along individual beach ridge crests into the late Holocene beach ridge complex of Figure 5a, site 3. Sites 6 and 8 can be projected along strike into the late Pleistocene chronostratigraphic sequence II_A of Figure 5a, sites 5 and 7. Site 12 can be projected along strike into the late Pleistocene chronostratigraphic sequence II_B of Figure 5b, sites 9, 10, 11, and 13.

CODE	G_1	$G_{2\,t\,\&\,p}$	S_1	$S_{2\,t\,\&\,p}$	$S_{3\,p\,\&\,d}$	S_4
SYMBOL						
NAME	Massive or crudely bedded sandy congl.	Cross bedded sandy congl.	Plane bedded pebbly sands	Cross bedded pebbly sands	Coarse plane bedded (p) or deformed (d) sands	Fine, plane bedded sands
COLOR	AWT: grayish orange; BWT: pale brown	Pale gray	Light olive gray to dark yellowish brown	Light olive gray to dark yellowish brown	Light olive gray to dark yellowish brown	Light olive gray to dark yellowish brown
GRAIN SIZE	Pebble congl. with coarse sand	Pebble congl. to very coarse sand	Coarse to granule sand with pebble stringers	Coarse to granule sand	Coarse to very coarse sand	Very fine to fine sand
INTERNAL BEDFORMS	Subhorizon. interstrat. coarse sand & pebble congl.; Lenticular to medium thick beds (Note 1)	Medium to thick lensatic beds. Matrix supported congl. (Notes 1 & 2)	Low angle laterally continuous wedge sets; medium to thick, concave upwards	Large scale trough (t) or planar (p) cross bedding	Decimeter thick tabular or wedge sets; massive or parallel laminated	Laterally extensive tabular or wedge-shaped beds comprised of thin to thick parallel lam.
NOTES	1. Clasts are intraformational mudballs (black symbols) or extraformational rocks (open symbols), the latter consisting of chert, vein quartz, olivine basalt, and micritic limestone.			2. G_2 bed continuity ranges from less than 1 m to across outcrop. Lenses subparallel to 2nd order truncation surfaces. Cross strata are either large scale low angle planar (p), or large scale (~ 1 m) cut and filled troughs.		

Figure 6. Symbols and facies description to accompany Figure 5.

imum and maximum (subunit B). Subunit C is not assigned a sea-level phase, owing to the lack of accurate age control.

Chronostratigraphic sequence I consists of extensive beach ridges (Figs. 5a and 5b) described in detail by Madrigal (1977), as well as fluvial terraces along major streams (Fig. 5b, site 4). The beach ridges step upward from modern sea level at the coast to ~10 m above mean sea level (Fig. 5a). The beach ridge sequence can be subdivided into a younger set of ridges with weakly developed soils (Cox, Bw horizons) and sharp topographic definition, and an older set with moderately developed soils (Bt horizons), degraded beach ridge morphology, and locations

TABLE 1. COMPILATION OF SAMPLE ATTRIBUTES, PACIFIC COAST, COSTA RICA

Sample identification*	Lambert grid coordinates†		Radiometric age (yr B.P.)§	Deposit depth (m)**	Azimuth and dip (in degrees)	Modern elevation (m)	Eustatic sea level (m)††
			Chronostratrigraphic sequence I				
Peninsula de Osa							
1-DIC-3154$_s$	Carate	541.8: 266.7	980 ± 40§§, †††	0 ± 2		4.3***	0
2-BETA-20836$_s$	Carate	542.7: 264.8	1390 ± 60§§,†††	0 ± 2		9	0 ± 1
3-BETA-20938$_s$	Carate	540.9: 272.2	2020 ± 60§§,†††	0 ± 2		4.6***	-1 ± 1
4a-BETA-24917$_w$	Golfo Dulce	536.7: 278.2	6350 ± 70†††	0 ± 2		5	-8 ± 1
4b-BETA-20841$_s$	Golfo Dulce	536.7: 278.2	7150 ± 80§§,†††	0 ± 2		4.5***	-14 ± 2
			Chronostratigraphic sequence II_A				
5-BETA-20838$_s$	Carate	540.4: 271.8	20140 ± 140§§	0 ± 2		13.4***	-103 ± 10
6-BETA-20837$_s$	Carate	542.3: 270.2	22210 ± 290	9 ± 6	170,9NE	12	-65 ± 12
7-DIC-3362$_s$	Carate	540.8: 271.9	22730 + 940 - 1060	9 ± 6	135,6NE	10.0***	-57 ± 13
8-BETA-24919$_w$	Carate	541.4: 267.5	26770 ± 1130	>15	120,14NE	5	-38 ± 7
			Chronostratigraphic sequence II_B				
9a-BETA-20941$_s$	Golfo Dulce	531.3: 276.5	29780 ± 1800§§	9 ± 6	140,5NE	40	-45 ± 10
9b-DIC-3153$_w$	Golfo Dulce	531.3: 276.5	34530 + 1210 - 1420	9 ± 6	140,5NE	40	-67 ± 8
10-BETA-24918$_s$	Golfo Dulce	528.3: 278.3	30720 ± 740	9 ± 6		50	-48 ± 6
11-BETA-20840$_s$	Golfo Dulce	536.2: 277.9	33070 ± 520	0 ± 2		7	-61 ± 6
12-BETA-24914$_s$	Gulfo Dulce	538.4: 273.9	34880 ± 510	9 ± 6	150,4NE	25	-68 ± 4
13-BETA-26780$_s$	Gulfo Dulce	524.3: 277.7	35290 ± 620§§	9 ± 6	140,7NE	40	-68 ± 4
			Chronostratigraphic sequence II_C				
14-BETA-25344$_s$	Gulfo Dulce	526.7: 277.5	>34,620	9 ± 6	120,24NE	95	
15-BETA-20839$_s$	Golfo Dulce	526.4: 277.7	>40,040	9 ± 6	110,28NE	110	
Peninsula de Nicoya							
N-BETA-20843$_s$	Matapalo	337.5: 257.5	1680 ± 60§§,†††	0 ± 2		2.7***	0 ± 1
Peninsula de Burica							
B-BETA-24922$_s$	Burica	587.9: 221.7	830 ± 50§§,†††	0 ± 2		3.9***	0 ± 1

*Example: for identification code 1-DIC-3154$_s$, 1 is site number used in location map (Fig. 4), uplift path (Fig. 8), and uplift rate calculation (Fig. 9). DIC is laboratory code (DIC, Dicarb Radioisotope Co.; BETA, Beta Analytic Inc.); 3154 is laboratory number; subscript denotes type of material (s, shell; w, wood).

†Lambert Grid Costa Rica South Zone coordinates are listed for east-west coordinate, then north-south coordinate. Name listed is for 1:50,000–scale topographic map.

§Error is one standard deviation.

**Depositional depth is estimated from facies reconstruction in Figure 5.

††Calculated from equation 10 in Pinter and Gardner (1989). Error is one standard deviation. Values are rounded to the nearest whole number.

§§Age adjusted for ^{13}C. Stable carbon ratio is calculated relative to PDB-1 international standard. Adjusted age is normalized to -25 per mil ^{13}C.

***Modern elevation (relative to mean sea level) determined from transit survey. All others estimated from 1:50,000–scale topographic map.

†††Dendro-corrected after Ralph and Michael (1974).

S_5 f & i	M_1	M_2	M_3
Flaser (f) or interbedded (i) sands and muds	Pebbly muds	Muds with occasional sand stringers	Muds
olive gray	AWT: moderate brown; BWT: grayish olive	AWT: moderate brown; BWT: grayish olive	AWT: moderate brown; BWT: grayish olive
Fine sand with interbedded mud	Gravel in a mud matrix	Clay to coarse silt with fine sand lenses	Clay to coarse silt
Small scale crossbeds with mud flasers (f) or laminated with mud layers (i)	Crudely horizontally stratified	Sands are thickly laminated or wave rippled	Sands are thickly laminated or wave rippled
3. AWT: above the water table; BWT: below the water table. Other symbols are: root traces; erosional contact; marine bivalves or gastropods; wood.			

Figure 6. (*Continued*).

that are landward of and at higher elevations than the younger set (Bullard and others, 1988).

Deposits from the beach ridges and fluvial terraces are differentiated on the basis of their sedimentary facies. The gravel facies (Fig. 5a) associated with the beach ridges are noticeably lacking in silt and clay, are well stratified, in many cases show imbrication, and contain a diverse, thick-shelled bivalve and gastropod assemblage (T. Aguilar, personal commun.) reported in Pinter, 1988). The limestone clasts are typically biogenically bored. Gravels of the fluvial terraces are less well stratified and contain more silt and clay, and the limestone clasts are generally not bored. The sand facies of the beach ridges are well sorted, in many cases plane-parallel laminated, and less volumetrically important than in the fluvial terraces, where the sand occurs as ripple cross-stratified lenses. Muds and clays, rarely observed in the beach ridge strata (Fig. 5a, site 3), are a characteristic component of the fluvial terrace (Fig. 5a, site 7; Fig. 5b, site 4).

Water depth during deposition of the beach facies is estimated by comparison to modern environments on the peninsula. The silt-free, stratified, shelly gravel and sands are similar to deposits of the present beach ridge–runnel system (depth ~2 m), swashface (depth ~0 m), and berm (depth ~–2 m). Thus, the depth of these facies during deposition is given in Table 1 as 0 ± 2 m with respect to mean sea level (MSL). Of course, this assumes that local tidal range has been relatively constant over time.

Chronostratigraphic sequence II underlies sequence I along the coastal plain (Fig. 7); farther inland, it underlies the foothills of the mountainous core (Fig. 5b, sites 9, 10, 13, and 15; Fig. 7). The diagnostic facies of chronostratigraphic sequence II are interbedded, grayish-olive muds and brown, silty, medium- to fine-grained sands (M_2 and M_3 of Fig. 6). These facies are semilithified and jointed, and dip consistently to the northeast. Dip of beds increases from 4°–14° in chronostratigraphic sequences II_A and II_B to 28° in chronostratigraphic sequence II_C. The beds are in many cases quite fossiliferous, with a molluscan fauna less diverse and thinner walled than fauna in the gravel facies of chronostratigraphic sequence I. Pebbly mudstones are common (Fig. 5b, site 14), and even the true conglomerates (fig. 5b, site 11) contain more silt and clay than do their sequence I counterparts.

Most strata of chronostratigraphic sequence II are assigned to a shoreface environment, based upon the wave-rippled sandstone interbeds, low flow-energy indicators, and less diverse fauna. Some thicker, sharp-based sand beds that contain soft-sediment deformation structures are interpreted to be tempestites emplaced on the lower shoreface during storms. On the basis of the bathymetry of the modern shoreface, we assign a water depth to these deposits of 9 ± 6 m below MSL.

The remaining strata of sequence II, such as the lower half of site 11 (Fig. 5b), are interpreted to have been deposited in a low-energy, mangrove deltaic environment, similar to the mouths of the modern Rio Agujas and Rio Tigre (Fig. 4). These beds contain *in situ* mangrove roots and stumps and a greater quantity of silty gravel. We assume a water depth to these deposits of 0 ± 2 m with respect to MSL. In the next section, the elevation of these deposits at the time of deposition and their ages are used to constrain an uplift history.

UPLIFT HISTORY

Uplift rate may be expressed as the positive change in elevation of the land mass per unit time. This quantity may be calculated as

$$\text{uplift rate (m/ka)} = [\text{modern elevation (m)} + \text{depositional depth (m)} + \text{paleo–sea level (m)}]/\text{age (ka)}. \quad (1)$$

The parameters were derived as follows and are compiled in Table 1.

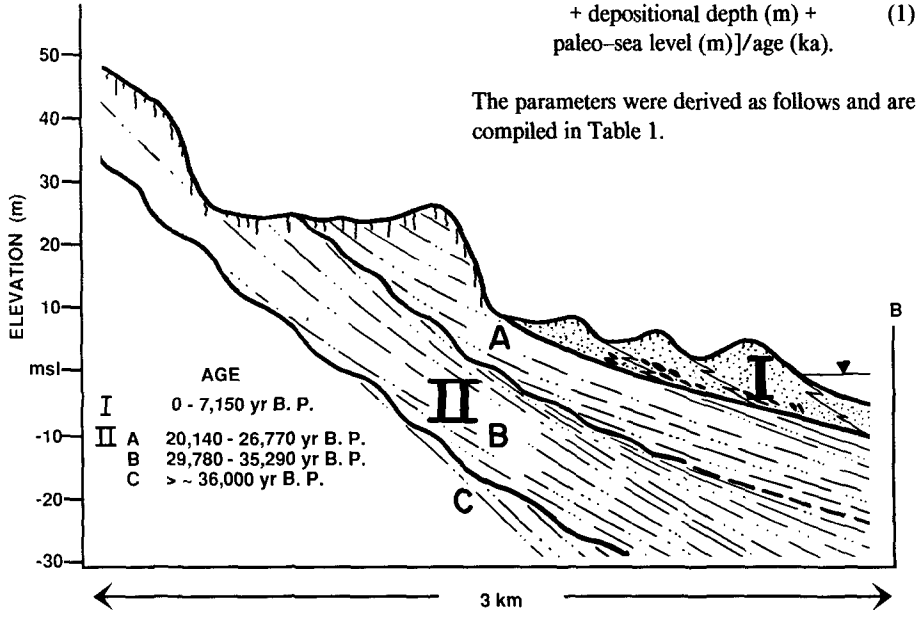

Figure 7. Generalized stratigraphic cross section drawn perpendicular to strike of bedding along the southeastern end of the Península de Osa (Fig. 4, line B), illustrating the relationships between chronostratigraphic sequences I and II.

(1) Age. The radiocarbon age of samples was determined by dating of either wood or shells. In nearly all cases for chronostratigraphic sequence II, articulated bivalves or complete gastropods were collected from unweathered interiors of joint blocks in the mudstones. Radiometric ages are internally consistent. For one location where multiple samples were collected (Fig. 5b, site 4), stratigraphically higher units are radiometrically younger. Furthermore, at closely spaced stratigraphic sections, radiometrically younger units are stratigraphically higher (Fig. 5a, sites 5 and 7). An age reversal occurs at only one location (Fig. 5b, site 9), indicating possible reworking of an older log into the stratigraphically younger unit.

(2) Site elevation. The modern elevation of sampling sites was determined by transit survey or from 1:50,000-scale topographic maps. Transit measurements are accurate to at least the nearest 0.1 m, whereas topographic-map elevations are reported to the nearest 1 m for areas with 10-m contours and to the nearest 5 m for areas with 20-m contours.

(3) Depositional depth. The depth below sea level at which the dated material was deposited was determined by facies analysis and paleoenvironmental reconstruction. The reconstructed environment was assigned a probable depth, according to commonly observed depths of such environments, with associated margins of uncertainty specified.

(4) Paleo-sea level. The height of the eustatic level of the oceans at the time of deposition of dated material is crucial to precise determination of uplift rates. For this purpose, we utilize a technique of polynomial interpolation (Pinter and Gardner, 1989) between dated and measured sea-level extrema from New Guinea (Bloom and others, 1974). The derived sea-level curve with error bars is generally quite consistent with a sea-level curve (0–18 ka) recently calculated for Barbados (Fairbanks, 1990). Importantly, the polynomial interpolation provides a single technique for estimating paleo-sea level and accompanying error bars for a sample of a given radiocarbon age for the entire range of our radiocarbon dates.

These four variables can be integrated into a graph of elevation versus time (Fig. 8), which includes the interpolated sea-level curve and points corresponding to all sampling localities along the eastern Península de Osa (Table 1). The x coordinate of each point is given by its radiocarbon age. The y coordinate is given by the elevation of the ocean at that age, less the depositional depth for that site. Error regions are designated as 1 standard deviation for sea level and age. The environmental range for depth of deposition is specified from facies reconstruc-

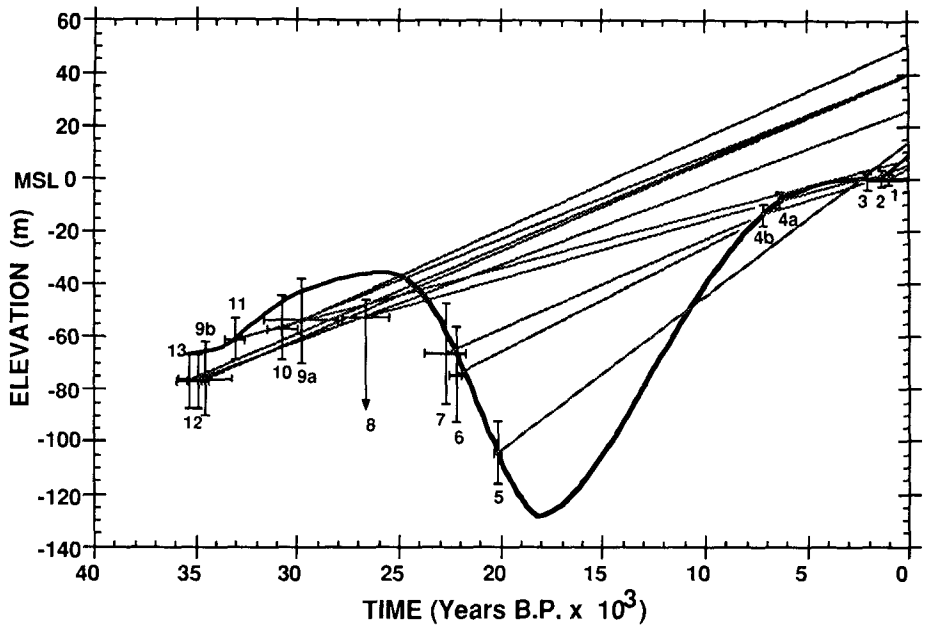

Figure 8. Plot of paleo-sea level (curved, solid line) from Pinter and Gardner (1989) and uplift paths (straight lines) for all dated samples on the Península de Osa. All data are reported in Table 1. Numbers beside points correspond to site numbers (Table 1, column 1). Horizontal error bar for age is from Table 1, column 3. Vertical error bar includes error for depositional depth from Table 1, column 4, and error for paleo-sea level from Table 1, column 7. The downward-pointing arrow for site 8 reflects the >15 m depositional depth for that sample.

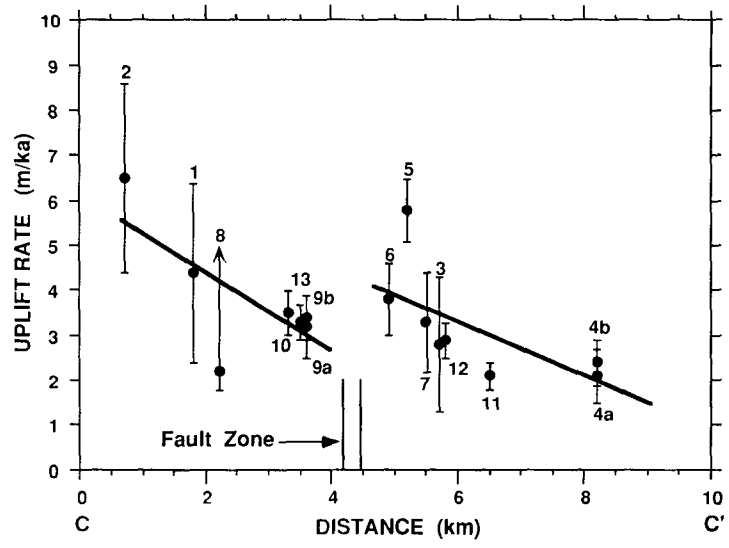

Figure 9. Calculated uplift rates with accompanying error bars for all dated sites on the Península de Osa. Numbers beside points correspond to site numbers (Table 1, column 1, and Fig. 4). Orientation and position of x axis are shown in Figure 4 inset, line C–C′. Distance along x axis is to the northeast along line C–C′. Vertical error bars include error in estimating age, depositional depth, and paleo-sea level. Position of fault zone is shown in Figure 4, line D. Linear regression equation is as follows. Uplift rate (m/ka) = 6.09 + –0.86x (r = 0.72), for $0 \leq x \leq 4.2$, and uplift rate (m/ka) = 7.03 + –0.62x (r = 0.63), for $4.2 \leq x \leq 8.2$, where x is distance along x axis.

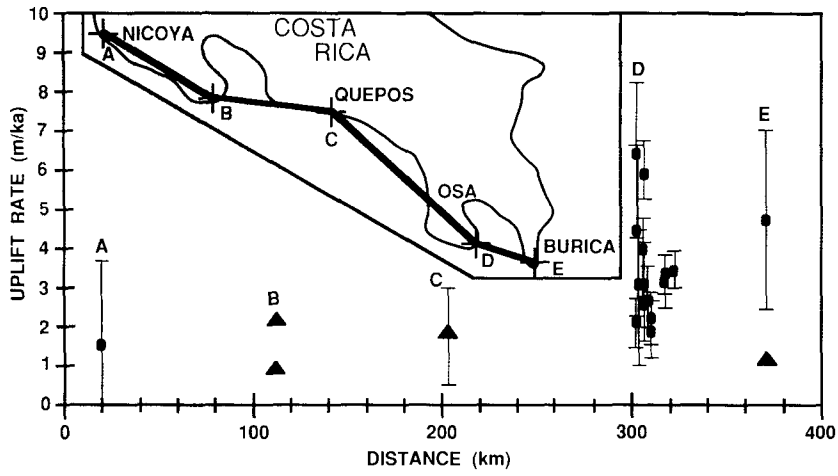

Figure 10. Uplift rates for a transect along the Pacific coast of Costa Rica for the Península de Nicoya (x axis at 100 km), Quepos (x axis at 200 km), the Península de Osa (x axis at 300 km), and the Península de Burica (x axis at 370 km). See Figure 1 for plate setting and bathymetry. Circles are for late Quaternary samples reported in Table 1. Triangles are for Pliocene, Pleistocene, and Holocene samples reported in the literature for which no error bars are reported (reported range is given for C).

tions. The modern elevation of each site is plotted on the y axis on the right side of the graph. Finally, the two points for each sampling site are connected by a straight line, which may be interpreted as the path of average uplift for that site.

The slope of each uplift path is the magnitude of the average uplift rate for that site over its postdepositional history. The relationship between the uplift path and the sea-level curve for a site is the emergence-submergence history of that site. Where the uplift path is above the eustatic curve for a given time interval, the model predicts that the site was subaerially exposed. The portion of the uplift path below the curve implies that the location was subaqueous during that time interval.

The straight-line uplift path may average higher uplift rates during short-term coseismic deformation with lower uplift rates during longer-term periods of tectonic quiescence. The straight-line uplift path, however, does represent a reasonable longer-term average that is supported by the data. Sites 4a and 4b (Fig. 8) lie along parallel, but slightly offset, uplift paths with the vertical separation equal to the thickness of the stratigraphic column between dated materials (Fig. 5b). The absence of $<\sim 10$ ka marine deposits in the stratigraphic columns for sites 8 and 13, and especially sites 6 and 7 (Fig. 5), suggests that those sites were not extensively resubmerged during sea-level rise after 18 ka. Thus, the slopes of those uplift paths (Fig. 8) could not have been much lower along the older portion of the path, or they would fall below the sea-level curve. The uplift path predicts submergence for site 5, but no marine deposits <10 ka were observed. Several kilometers to the northeast, however, Holocene beach ridge deposits do occur at or slightly above the elevation of the dated sample at site 5, indicating that it could have been submerged in the Holocene as the uplift path predicts. Given that the dynamic crustal model (described later) uses a 50,000-yr time step, the long-term average uplift rates calculated from the slope of the straight-line uplift path are appropriate.

If uplift rates were uniform both through time and along the peninsula, then all lines of uplift in Figure 8 would be parallel. Instead, there is scatter between sites. Because uplift rates calculated among sites of similar ages vary as widely as among sites of different ages, it is unlikely that the assumption of average uniform uplift through time is the source of the scatter.

The variation in uplift rate may be rationalized by orthogonally projecting the location of each site onto a transect that is perpendicular to both the trend of the Middle America Trench (Fig. 1) and the regional northwest strike of bedding in chronostratigraphic sequence II (Table 1, column 5). There is a relationship between geographic position and uplift rate, such that the highest uplift rates occur closest to the subduction zone and decrease inland (Fig. 9). Accordingly, the southwestern portion of the study area is being uplifted at a rate of ~ 6 m/ka, decreasing to 2 m/ka on the northeast coast along the Gulfo Dulce.

A zone of poorly exposed, northwest-striking, subvertical faults (Figs. 4 and 9) that are subparallel to the strike of bedding has been mapped in isolated outcrops along the foothills and coastal plain (Bullard and others, 1988). One high-angle, northeast-side-up fault cuts >35,900 yr B.P. sediments along the Río Platanareas southwest of site 5 (Fig. 4). This same fault apparently controls deposition of late Holocene beach ridges (Bullard and others, 1988). Another fault north of site 9 (Fig. 4) along the Río Tigre displaces 29,780–34,530 yr B.P. sediments. Observed stratigraphic offset of at least 1–2 m across these faults demonstrates that differential movement of discrete blocks does exist, although the magnitude of offset is less than that inferred for the fault zone in Figure 9. The sense of motion across the fault zone is consistent with a recent interpretation of high-angle, northeast-dipping, thrust faults along the Península de Osa (Kriz, 1990). Along the fault zone shown in Figure 9, however, northeast-side-up motion would elevate the coastal plain relative to the foothills, a condition generally not consistent with the modern topography. This would require that fluvial, and especially marine, planation has eroded the poorly consolidated beds on the upthrown side of the fault, creating the piedmont and coastal plain along the northeast side of the peninsula. Thus, deformation of this portion of the Península de Osa can be approximated as northeast-tilted fault blocks. The implication is that the area is actively being uplifted, block faulted, and tilted down to the northeast with an average angular velocity of $\sim 0.03°$ to $0.06°$ per thousand years.

Block faulting and regional down-to-the-northeast tilting of the Península de Osa are consistent with other data on the peninsula. For example, evidence of uplift on the Península de Osa has been difficult to reconcile with other evidence of subsidence only a few kilometers away in the Golfo Dulce (Lew, 1983). The model described herein predicts subsidence in the Gulfo Dulce offshore of the northeast coast of the peninsula. A study of watershed morphometry of the Península de Osa (Gardner and others, 1987) demonstrated systematic drainage-basin asymmetry that suggested down-to-the-northeast tilting into the Gulfo Dulce. Dips of beds, especially in chronostratigraphic sequence II, are consistent with block faulting and down-to-the-northeast tilting. Beds consistently strike northwest-southeast and dip to the northeast, and dip tends to increase with increasing age although somewhat inconsistently (Table 1, column 5). Poorly exposed faults observed in isolated outcrops in the foothills and coastal plain may be responsible for some of the locally steeper dips in chronostratigraphic sequence II_A. As a first approximation, however, deformation

of the Península de Osa can be described as uplifted and down-to-the-northeast–tilted fault blocks.

UPLIFT HISTORY–PENÍNSULA DE NICOYA, QUEPOS, AND PENÍNSULA DE BURICA

Calculated uplift rates for other sites along the Pacific coast in a transect perpendicular to the Cocos Ridge (Fig. 10) are less well constrained than for the Península de Osa, but do provide estimates of uplift rates with distance from the Cocos Ridge. These data suggest a decrease in uplift rate with distance from the Cocos Ridge. Late Quaternary uplift rates are calculated for two locations on the Península de Nicoya, ~200 km to the northwest of the Cocos Ridge (Fig. 1). A sample from an elevated beach ridge at Playa de Tamarindo (Table 1, Península de Nicoya) on the northwestern portion of the peninsula, with a radiometric age of 1680 ± 60 yr B.P., yields an uplift rate of 1.6 ± 2.0 m/ka. Bergoeing (1983) reported a 6620 ± 150 yr B.P. age for a 7-m terrace at Montezuma on the southern tip of the peninsula. Allowing for a 10-m sea-level depression at that time (Pinter and Gardner, 1989) yields an uplift rate of ~2.5 m/ka. Recent work on Holocene beach ridges on the Península de Nicoya indicated a regional northeastward tilt of 1.7 m/km along the southwestern margin of the peninsula (Anderson and others, 1989). Longer-term uplift rates can be estimated from elevation of the Pliocene (McKee, 1985) to early Pleistocene (Lundberg, 1982; Baumgartner and others, 1984; Chinchilla, 1988) Montezuma Formation exposed along the southeastern tip of the peninsula. If one assumes a maximum water depth of 300 m from facies reconstruction (Lundberg, 1982) and benthic foraminifera (McKee, 1985), and a modern average elevation of ~200 m, the average uplift rate is <1 m/ka, slightly less than the shorter-term, late Quaternary uplift rate. All three estimates, however, are significantly less than the maximum uplift rate on the Península de Osa. Given the regional down-to-the-northeast tilting inferred by Anderson and others (1989), the sample sites located on the southwestern coastline of the Península de Nicoya would tend to be maximum values, yet still are less than the maximum uplift rates on the Península de Osa. This further supports our contention that uplift rates decrease away from the Cocos Ridge.

Average incision rates of fluvial systems have been used to calculate late Quaternary uplift rates (Drake, 1989) in the Quepos region midway between the Península de Nicoya and the Península de Osa (Fig. 10). Elevation above local base level of five post–34,000 yr B.P. terraces yields uplift rates ranging from 0.5 to 3.0 m/ka. This range of uplift brackets the uplift rates on the Península de Nicoya but is less than half the maximum uplift rates for the same time interval on the Península de Osa.

A late Quaternary uplift rate of 4.7 ± 2.0 m/ka is estimated for an 830 ± 50 yr B.P. wave-cut platform 3.9 m above mean sea level (Table 1) on the southern tip of the Península de Burica, ~60 km to the southeast of Osa. This is within the range for the maximum late Quaternary uplift rates at Osa, but significantly above the longer-term rate of 1.2 m/ka calculated from uplift of late Pliocene, deep-water sediments on the Península de Burica (Corrigan and Mann, 1986).

In the next section, uplift rates for sites on the Península de Osa are used to constrain a geodynamic model for the Quaternary subduction of the aseismic Cocos Ridge and uplift of the overriding Caribbean plate. The constrained geodynamic model is then used to predict uplift rates along the Pacific coast that can be attributed to subduction of the Cocos Ridge.

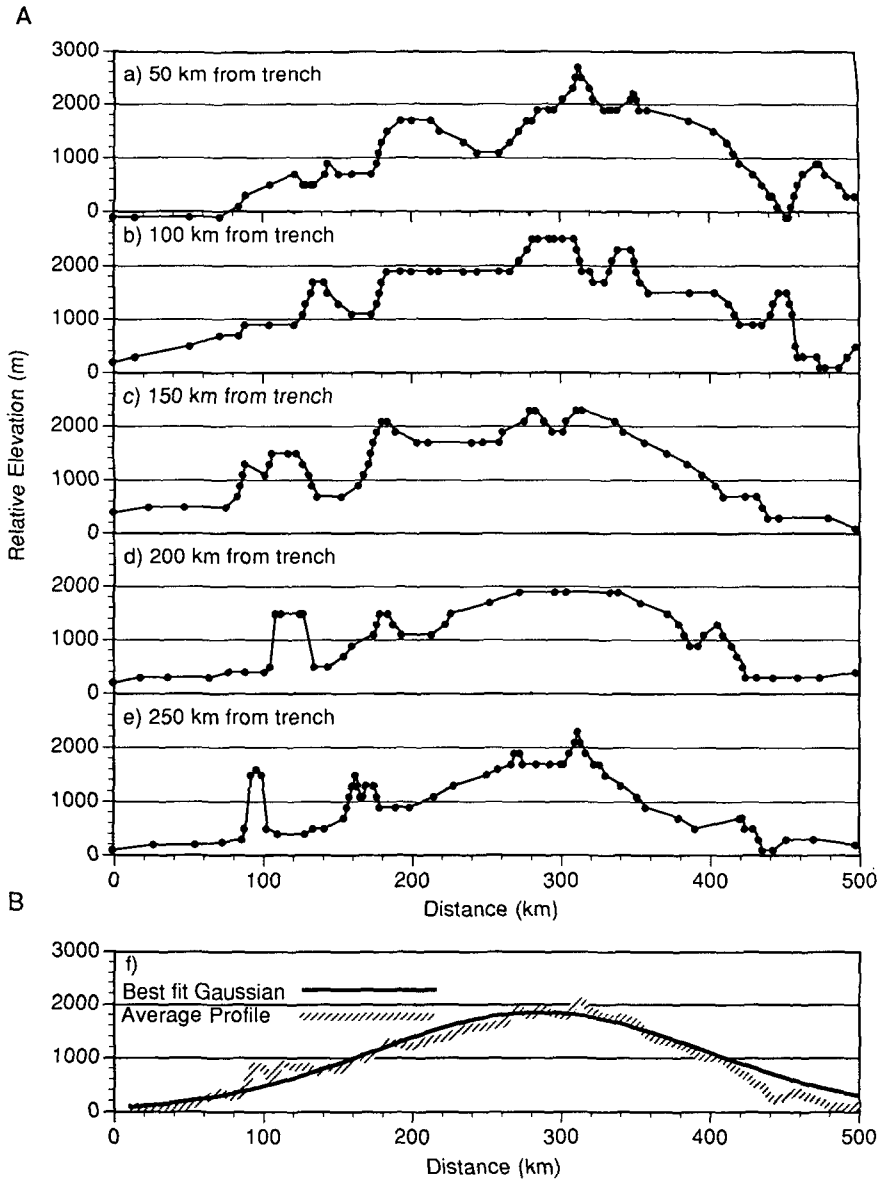

Figure 11. Bathymetric cross section of the Cocos Ridge perpendicular to the strike of the ridge. The bottom section shows the average elevation of the Cocos Ridge relative to the adjacent basins. Values shown are elevation relative to the average depth of the adjacent basin. See Figure 1 for cross-section locations.

GEODYNAMIC MODEL

Buoyancy of the Cocos Ridge

Our intention in this section is to use a geodynamic model that is constrained by the observed uplift rates on the Península de Osa to explore the fundamental cause of uplift, but not specific faulting scenarios. We examine two end-member bathymetric models of the Cocos Ridge and a range of effective elastic thicknesses for the overriding Caribbean plate. Here, we utilize the elastic model of Moretti and Ngokwey (1985), where the overriding lithosphere is assumed to behave as a perfectly elastic plate that is deflected upward by the buoyancy of a subducting ridge. Moretti and Ngokwey (1985) rejected horizontal compression due to ridge collision as a cause of deformation in the overriding plate because it required an unrealistic horizontal stress. Therefore, we consider only the vertical stress caused by the buoyancy of the aseismic Cocos Ridge.

The aseismic Cocos Ridge is a broad shallow bathymetric feature, ~2,000 m shallower than the adjacent basin (Fig. 1). Refraction and gravity data indicate that the shallow bathymetry of the Cocos Ridge is due to a low-velocity, low-density supracrustal volcanic layer ~2 km thick that is compensated by a thickened oceanic crust (Bentley, 1974). The low-density volcanic rock and thick crustal root make the Cocos Ridge more buoyant than the adjacent Cocos plate. Because the rate and direction of convergence are similar for the Península de Osa, Península de Nicoya, and Península de Burica regions, the differences in subduction can be attributed fundamentally to the buoyancy of the aseismic Cocos Ridge. Figure 11 shows five bathymetric cross sections of the Cocos ridge at 50-km intervals beginning 50 km from the trench. The cross sections were generated by interpolating (cubic spline) between unevenly spaced bathymetric contours (Case and Holcombe, 1980). A mathematical expression for the bathymetry was calculated as a Gaussian curve that was fit to the average of the five cross sections (Fig. 11f). The Gaussian shape was used in the dynamic model. Because the shape of the subducted end of the Cocos Ridge is unknown, two bathymetric models are proposed. (1) The subducted end of the ridge is radially symmetric (Gaussian shape) with a slope similar to the slope of the flanks of the observable portion of the ridge (Fig. 12, model 1), and (2) the subducted end of the ridge terminates abruptly where it was truncated by the Panama fracture zone (Figs. 3 and 12, model 2).

The buoyant load $S(x,y)$ per unit area at any point can be expressed as the elevation relative to the basin $\Delta h(x,y)$, multiplied by the difference in density of the overlying and underlying fluids and the gravitational acceleration, g:

$$S(x,y) = \Delta h(x,y)(\rho_u - \rho_o)g. \quad (2)$$

The load applied to the overriding plate is calculated from equation 2, using the elevation differences from each of the two bathymetric models, a mantle density (ρ_u) of 3,300 kg-m^{-3}, and a density for the overlying fluid of water (ρ_o), 1,000 kg-m^{-3}. The maximum buoyant load corresponds to the shallowest bathymetry and is approximately 46 MPa for both bathymetric models.

Elastic Flexure Model

In the elastic flexure model, we assume that the lithosphere of the overriding plate at subduction zones behaves as a continuous, isotropic, homogeneous elastic plate overlying a fluid mantle. The lithospheric plate is deformed by forces associated with an underthrusting buoyant aseismic ridge, similar to the model used by Moretti and Ngokwey (1985) to describe the subduction of the Entrecasteaux fracture zone at the New Hebrides Trench. The deflection, w, of a perfectly elastic plate embedded in a fluid, neglecting horizontal forces, is given by

$$D\nabla^4 w + (\rho_u - \rho_o)gw = F \quad \text{(Walcott, 1970),} \quad (3)$$

where g is the gravitational acceleration; ρ_u and ρ_o are the densities of the underlying and overlying fluids, respectively; F is the applied vertical force; and D is the flexural rigidity defined as

$$D = Eh^3/[12(1 - \sigma^2)], \quad (4)$$

where E is Young's modulus, h is the elastic thickness, and σ is Poisson's ratio. Because the plate is perfectly elastic, the deflection from individual point loads can be summed to give the total deflection. A first-order approximation for the deflection can be found using an infinite-plate model (Moretti and Ngokwey, 1985). Moretti and Ngokwey (1985) applied an upward load throughout an area of contact between the subducting and overriding plates, which extended from the trench to the subducted end of the ridge. Their model, however, severely underestimated the uplift near the trench. To avoid that problem in the present model, the contact zone was taken to extend from the subducted end of the ridge seaward to infinity. This is necessary because the overriding plate is modeled as an infinite plate that also extends seaward.

The analytic solution for equation 3 for an infinite plate under a point load is

$$w = F/[(\rho_u - \rho_o)\pi g\alpha^2]\ \mathrm{kei}_o(r\sqrt{2}/\alpha) \quad \text{(Moretti and Ngokwey, 1985),} \quad (5)$$

where r is the radial distance from the point load, kei_o is the zero-order Kelvin function, and α is the flexural parameter defined as

$$\alpha^4 = 4D/[(\rho_u - \rho_o)g]. \quad (6)$$

The force applied to the overlying plate is caused by the buoyancy of the aseismic ridge and can be represented as point loads distributed throughout an area of contact between the ridge and the overriding plate. The vertical force, F, is the vertical stress, S, divided by the number of points per unit area. The deflection at any point on the plate due to each point load is calculated from equation 5. The uplift rate is then calculated by determining the change in total deflection with time as the ridge continues to be subducted.

Flexural Uplift along the Pacific Coast of Costa Rica

Uplift along the Pacific coast of Costa Rica is modeled by calculating the deflection of an elastic plate caused by the upward force produced

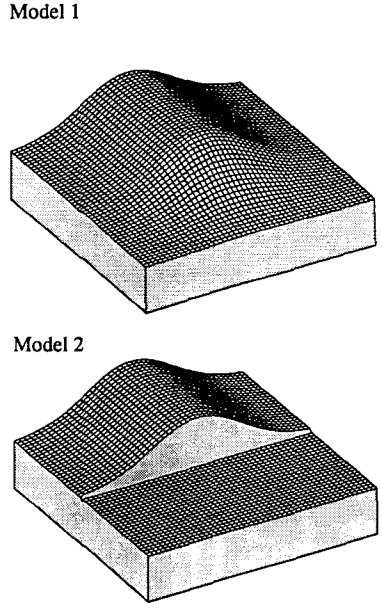

Figure 12. Two bathymetric models for the subducted end of the Cocos Ridge. In model 1, the subducted end of the ridge is radially symmetric, and in model 2, the subducted end of the ridge terminates abruptly.

by the subduction of the buoyant Cocos Ridge. The deflection is calculated for two extreme cases (Fig. 12), a radially symmetric ridge (model 1) and a truncated ridge (model 2). The overriding Caribbean plate is divided into a 500-km-square grid with a 5-km grid spacing. The deflection of each point on the Caribbean plate is calculated for each point load produced by the Cocos plate and then summed over all the points of the Cocos plate to find the total deflection. The uplift rate along the Pacific coast of Costa Rica is calculated for a 50,000-yr time period using a convergence rate of 95 mm-yr^{-1} (Minster and Jordan, 1978). Both bathymetric models include as assumptions a Poisson's ratio, σ, of 0.25 and Young's modulus, E, of 80 GPa, based on a basaltic composition of the elastic plate.

The effective elastic thickness of continental lithosphere has been estimated to range from >5 to <60 km (Banks and others, 1977; McNutt and Parker, 1978; Haxby and others, 1976; Cochran, 1980), with corresponding flexural rigidities ranging from 8×10^{20} to 1.5×10^{24} N-m^{-2} and flexural parameters of ~20 to 125 km. Maximum uplift rates on the Península de Osa, immediately landward of the Cocos Ridge, are calculated for several Caribbean plate effective elastic thicknesses for each bathymetric model (Table 2). Model 1 predicts that the maximum uplift rate occurs in an almost circular region inland of the Península de Osa with absolute values much less than observed values (Fig. 10) for all effective elastic thicknesses. For model 2 with an effective elastic thickness of 5 km, the uplift rate for the Península de Osa region approaches the range of observed uplift rates on the Península de Osa (Fig. 10) and occurs in a narrow region directly above the subducted end of the ridge. Both models predict that the region of fastest uplift becomes larger as the effective elastic thickness increases. The maximum rate, however, decreases.

The uplift rate is affected by the buoyant force, the convergent rate, and the effective elastic thickness of the overriding plate. Model 1 would require a stress of at least 200 MPa to produce maximum uplift rates consistent with the observed uplift. This is more than 4 times greater than the buoyant stress indicated by the bathymetry of the Cocos Ridge. Thus model 1 is an unlikely situation and is not investigated further.

Model 2 yields acceptable uplift rates for the Pacific coast of Costa Rica if the effective elastic thickness of the Caribbean plate is approximately 5 km. The total uplift and uplift rate calculated for an effective elastic thickness of 5 km are shown in Figure 13 for a coastal section from the Península de Burica to the Península de Nicoya. The highest uplift rate occurs almost directly over the subducted end of the Cocos Ridge above the Península de Osa. The calculated values best fit the observed data when the Cocos Ridge began to be subducted, about 0.5 Ma, or equivalently, when the subducted end of the Cocos Ridge had penetrated 50 km beneath the Caribbean plate, about 60% of that estimated from plate reconstructions. From this model, the predicted uplift rate perpendicular to the trench across the Península de Osa (Fig. 14A) best fits observational data. This yields a pattern of uplift that would produce a northeast tilting of the Península de Osa and areas of subsidence northeast of the Gulfo Dulce that are also consistent with observations. Figure 14B shows the observed and predicted uplift rate parallel to the trench along the Costa Rica coastline. The model predicts a decrease in uplift rate away from the Cocos Ridge. Model predictions fall between the range of observed values for Burica and southernmost Nicoya and allow for the observed northeastward tilt of Holocene beach ridges along the southeastern coast of the Península de Nicoya (Anderson and others, 1989). Predicted uplift is low, but within the error range for the northwesternmost Nicoya sample. Given that the model transect lies seaward of the Quepos region, the model actually predicts negligible uplift for that region. The observed uplift would therefore result from processes other than buoyancy of the subducted ridge, possibly subduction of seamounts or the accretionary prism along the Middle America Trench, or isostatic rebound in response to denudation.

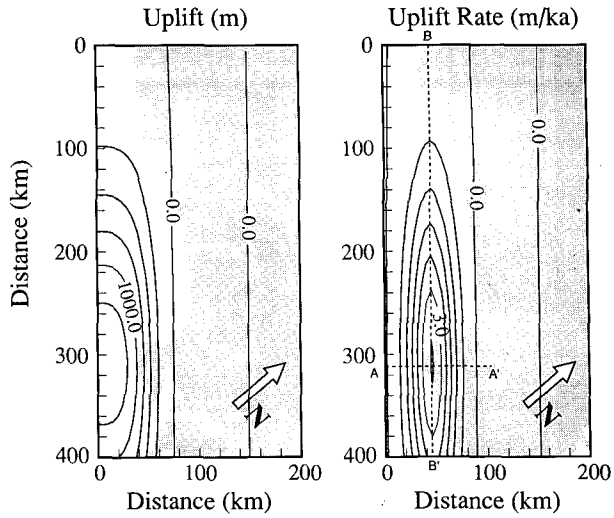

Figure 13. Contour plots of calculated total uplift and uplift rate where the Cocos Ridge has penetrated 50 km, or equivalently has been subducted for 0.5 m.y., beneath the overriding Caribbean plate with an effective elastic thickness of 5 km.

TABLE 2. MAXIMUM UPLIFT RATE FOR THE PENÍNSULA DE OSA CALCULATED FOR DIFFERENT EFFECTIVE ELASTIC THICKNESSES (EET)

	Maximum uplift rate (m/ka)	
EET (km)	Model 1	Model 2
5	0.96	3.72
10	0.81	2.10
20	0.69	1.20
30	0.54	0.81

Discussion of Flexural Model

Model 2 gives a first-order estimate of the observed uplift rate and the angular rotation along the Pacific coast of Costa Rica that can be attributed to buoyance of the subducting Cocos Ridge. It is based on the assumptions that the subducted end of the Cocos Ridge ends abruptly and that the flexural rigidity of the Caribbean plate in this region is on the order of 10^{20} N-m^{-2}. McNutt and Parker (1978) have successfully modeled the flexure of continental lithosphere, using a flexural rigidity as low as 2×10^{19} N-m^{-2}, indicating that an effective elastic thickness of 5 km is reasonable for this region of Central America. The model could be further improved by approximating the overriding plate as a semi-infinite plate and by accounting for the elastic response of the subducting plate. The assumption concerning the shape of the subducted end of the Cocos Ridge in model 2 suggests an extreme case where the original ridge was orthogonally truncated by the Panama fracture zone and ends as a vertical wall. As a first approximation, orthogonal truncation was utilized to accommodate the grid orientation in the geodynamic model. The Panama fracture zone actually truncates the Cocos Ridge at an oblique angle (Fig. 3). Using a diagonally truncated Cocos Ridge in the geodynamic model would not significantly affect the magnitude of the total uplift or uplift rate (Fig. 13), but would tend to rotate the axes of the ellipses defined by the uplift rate contours farther inland in the direc-

tion of the Península de Nicoya. This would yield model results that are more consistent with the observed uplift rate in the Quepos region. A vertical wall may be unrealistic, but we suggest that the subducted end of the ridge is likely to have had a much steeper slope than the sides of the ridge, because it was truncated by the Panama fracture zone (Fig. 3). A ridge with a vertical face would most likely push up sediments in the accretionary wedge during subduction. Surface uplift caused by deformation within such a wedge, however, is much less than observed uplift on the Península de Osa (Verdonck, 1989).

The uplift rate varies significantly along the Pacific coast of Costa Rica. We submit that this variation in uplift rate is directly related to the subduction of the Cocos Ridge in the vicinity of the Península de Osa. Our model indicates that the subducted end of the Cocos Ridge likely had a steep slope and that the crest of this leading end has penetrated ~50 km beneath the Caribbean plate. The buoyancy of the Cocos Ridge causes it to subduct at a low angle, which is evident in the lack of deep seismicity beneath the Península de Osa (Fig. 2c). Although there is very little seismic activity directly beneath the Península de Osa, shallow, subduction-related seismicity is present farther inland (Adamek and others, 1987). This activity may be associated with either deformation in the overriding plate or movement of lithosphere subducted prior to subduction of the Cocos Ridge.

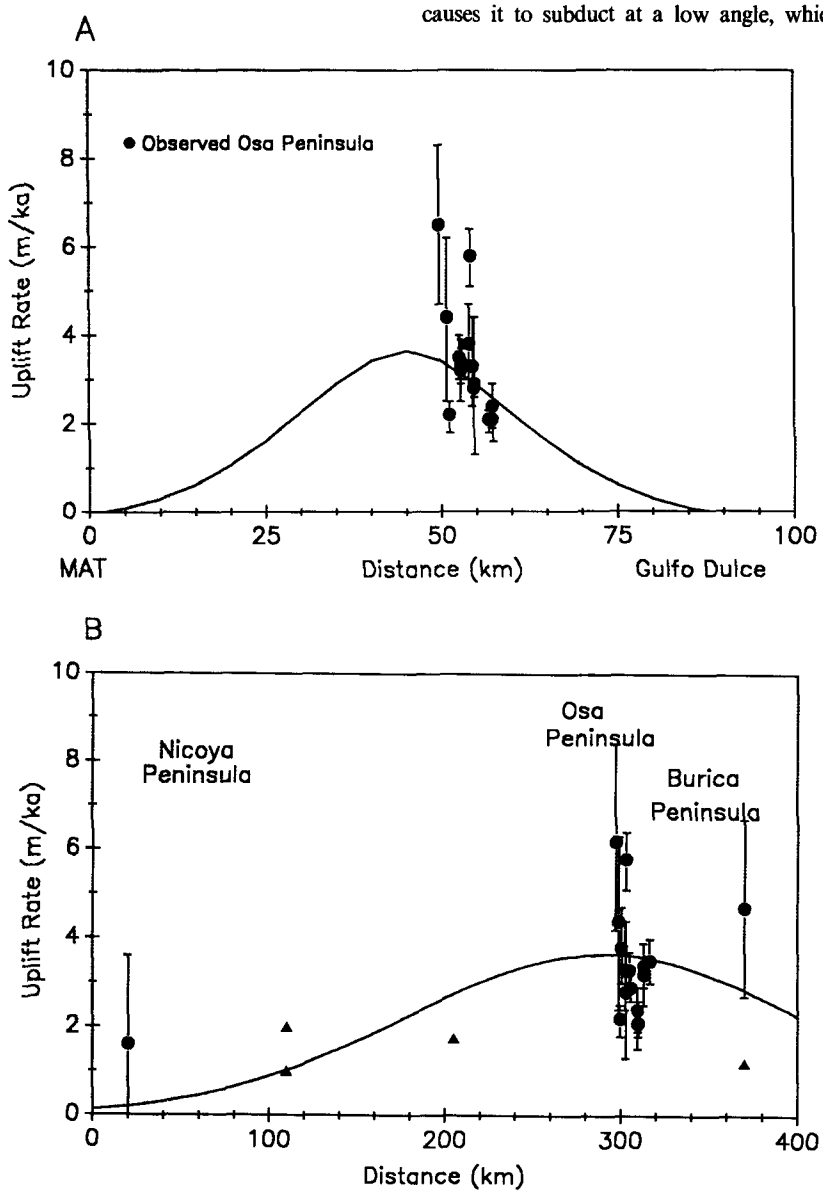

Figure 14. Observed (solid symbols from Fig. 10) and predicted (solid line) uplift rate, using bathymetric model 2 for the Pacific coast of Costa Rica. A–A′, uplift rate perpendicular to the Middle America Trench across the Península de Osa. B–B′, uplift rate parallel to the Middle America Trench along the Costa Rica coastline crossing the Península de Burica, Península de Osa, and Península de Nicoya. See Figure 13 for exact locations. Projection of uplift rate values to less than zero (not shown) indicates subsidence.

CONCLUSIONS

The Pacific coast of Costa Rica parallels the Middle America Trench and lies astride the aseismic Cocos Ridge. It is ideally situated for an analysis of crustal uplift that results from subduction of the Cocos Ridge. The Pliocene and Pleistocene stratigraphic record and Holocene marine terraces and beach ridges indicate that the highest, maximum rates of crustal uplift have occurred on the Península de Osa, immediately landward of the Cocos Ridge. Although less well constrained, crustal uplift rates decrease toward the Península de Nicoya, 200 km to the northwest, and to a lesser extent toward the Península de Burica, 60 km to the southeast.

On the Península de Osa, the late Quaternary stratigraphy is subdivided into two chronostratigraphic sequences, based on radiocarbon ages. Chronostratigraphic sequence I consists of a middle to late Holocene (<7150 yr B.P.) beach ridge complex, whereas chronostratigraphic sequence II consists of late Pleistocene (20,140 to >36,000 yr B.P.) shallow-marine to deltaic, mangrove units. Uplift rates on the Península de Osa calculated from these sequences vary from a maximum of 6.5 m/ka in the southwest along the axis of the peninsula to <2.1 m/ka in the northeast along the Gulfo Dulce. Deformation of the Península de Osa is approximated as uplifted and down-to-the-northeast–tilted blocks, with an angular velocity of ~0.03° to 0.06° per thousand years for at least the past 35 ka. This deformation style is consistent with ancillary data from strike and dip directions of late Pleistocene marine units and drainage-basin asymmetries.

On the Península de Nicoya, uplift rates vary from 2.5 to 1.6 m/ka for Holocene terraces to <1 m/ka for the Pliocene and Pleistocene Montezuma Formation. In the Quepos region, uplift rates measured from late Quaternary fluvial terraces range from 0.5 to 3.0 m/ka. On the Península de Burica, significantly closer to the aseismic ridge, calculated uplift rates vary from a maximum of 4.7 m/ka for the latest Holocene to 1.2 m/ka for the post-late Pliocene.

A geodynamic model is used to calculate the vertical deformation of the overlying Caribbean plate where that plate is assumed to behave as a

perfectly elastic plate deflected upward owing to the buoyancy of the subducting Cocos Ridge. The best-fit bathymetric model utilizes an abruptly truncated Cocos Ridge that has been subducted ~50 km beneath the overriding Caribbean plate. The Caribbean plate has a flexural rigidity of approximately 10^{20} N-m^{-2} and an effective elastic thickness of 5 km. The model predicts a maximum uplift rate of 3.7 m/ka along the southwest coast of the Península de Osa, slightly less than the average observed value. It reproduces the observed northeast tilting of the peninsula and the decrease in uplift rates along the coast away from the Cocos Ridge.

ACKNOWLEDGMENTS

We are most grateful to Sr. F. M. Rudin (Director, Instituto Geográfico Nacional) for providing logistical support, to Dr. S. Mora C. (Instituto Costarricense de Electricidad), and to Dr. Teresita Aguilar (Universidad de Costa Rica) for stimulating geologic discussions and field trips. We thank *Bulletin* reviewers R. Anderson, W. Lettis, M. Lisowski, D. Schwartz, and G. Valensise for substantive and helpful reviews of early drafts. Funding was provided by National Science Foundation Grants EAR86-15277 (TWG, KPF, and RS) and EAR86-16779 (SGW). Effort was directed toward primary responsibility for field work (TWG, NMP, RS, TFB, and SGW) and for dynamic modeling (DV and KPF).

REFERENCES CITED

Adamek, S., Tajima, F., and Wiens, D. A., 1987, Seismic rupture associated with subduction of the Cocos Ridge: Tectonics, v. 6, p. 757–774.

Alt, J. N., Harpster, R. E., and Schwartz, D. P., 1980, Late Quaternary deformation and differential uplift along the Pacific coast of Costa Rica: Geological Society of America Abstracts with Programs, v. 12, p. 378–379.

Anderson, R. S., Marshall, J. S., and Brenes, J. A., 1989, Evidence of repeated coseismic uplift along the southern coast of Nicoya Peninsula, Costa Rica: Geological Society of America Abstracts with Programs, v. 21, p. A92.

Astiz, L., and Kanamori, H., 1984, An earthquake doublet in Ometepec, Guerrero, Mexico: Physics of the Earth and Planetary Interiors, v. 34, p. 24–45.

Banks, R. J., Parker, R. L., and Huestis, S. P., 1977, Isostatic compensation on a continental scale: Local versus regional mechanisms: Royal Astronomical Society Geophysical Journal, v. 51, p. 431–452.

Barritt, S., and Berrangé, J. P., 1987, Interpretation of a gravity survey of the Osa Península and environs, southern Costa Rica: British Geological Survey Overseas Geology and Mineral Resources Publication 65, 19 p.

Baumgartner, P. O., Mora, C., Butterlin, J., Sigal, J., Glacon, G., Azéma, J., and Bourgois, J., 1984, Sedimentación y paleogeografía del Cretácio y Cenozoico del litoral Pacífico de Costa Rica: Revista Geológica de América Central, v. 1, p. 57–136.

Bentley, L. R., 1974, Crustal structure of the Carnegie Ridge, Panama Basin and Cocos Ridge [M.S. thesis]: Honolulu, Hawaii, University of Hawaii, 49 p.

Bergoeing, J. P., 1983, Dataciones radiométricas de algunas muestras de Costa Rica: Instituto Geográfico Nacional Informe Semestral, Enero y Junio, p. 71–86.

Bloom, A. L., Broecker, W. S., Chappell, M. A., Mathews, R. K., and Mesolella, K. J., 1974, Quaternary sea level fluctuation on a tectonic coast: New $^{230}Th/^{234}U$ dates from the Huon Peninsula, New Guinea: Quaternary Research, v. 4, p. 553–570.

Bourgois, J., Azéma, J., Baumgartner, P. O., Tournon, J., Desmet, A., and Ouboin, J., 1984, The geologic history of the Caribbean-Cocos plate boundary with special reference to the Nicoya Ophiolite complex (Costa Rica) and D.S.D.P. results (Legs 67 and 84 off Guatemala); A synthesis: Tectonophysics, v. 108, p. 1–32.

Bullard, T. F., Wells, S. G., Gardner, T. W., Pinter, N., and Slingerland, R., 1988, Geomorphic and pedogenic evolution of an emergent coastal piedmont, Osa Peninsula, Costa Rica: Implications for latest Quaternary tectonism and fluvial adjustments: Geological Society of America Abstracts with Programs, v. 20, p. A55.

Burbach, G. V., Frohlich, C., Pennington, W. D., and Matumoto, T., 1984, Seismicity and tectonics of the subducted Cocos plate: Journal of Geophysical Research, v. 89, p. 7719–7735.

Case, J. E., and Holcombe, T. L., 1980, Geologic and tectonic map of the Caribbean region: U.S. Geological Survey Miscellaneous Investigation Map I-1100.

Chinchilla, A., 1988, Estudio geológico estratigráfico de la Formación Montezuma, Península de Nicoya, Costa Rica [thesis]: San José, Costa Rica, Universidad de Costa Rica, 120 p.

Chung, W., and Kanamori, H., 1978, A mechanical model for plate deformation associated with aseismic ridge subduction in the New Hebrides arc: Tectonophysics, v. 50, p. 29–40.

Cochran, J. R., 1980, Some remarks on isostasy and the long-term behavior of the continental lithosphere: Earth and Planetary Science Letters, v. 46, p. 266–274.

Corrigan, J. C., and Mann, P., 1986, Rapid outer-forearc uplift related to attempted subduction of an aseismic ridge: The Burica Peninsula, Panama–Costa Rica: Geological Society of America Abstracts with Programs, v. 18, p. 571–572.

Corrigan, J. C., Mann, P., and Ingle, J. C., 1990, Forearc response to subduction of the Cocos Ridge, Panama–Costa Rica: Geological Society of America Bulletin, v. 102, p. 628–652.

Cross, T. A., and Pilger, R. H., 1982, Controls of subduction geometry, location of magmatic arcs, and tectonics of arc and back-arc regions: Geological Society of America Bulletin, v. 93, p. 545–562.

Drake, P. G., 1989, Quaternary geology and tectonic geomorphology of the coastal piedmont and range, Puerto Quepos area, Costa Rica [M.S. thesis]: Albuquerque, New Mexico, University of New Mexico, 183 p.

Fairbanks, R. G., 1989, A 17,000-year glacio-eustatic sea level record: Influence of glacial melting rates on the Younger Dryas event and deep-ocean circulation: Nature, v. 342, p. 637–642.

——1990, U-Th ages obtained by mass spectrometry in corals from Barbados: Sea level during the last 130,000 years: Nature, v. 346, p. 456–458.

Gardner, T. W., Back, W., Bullard, T. F., Hare, P. W., Kesel, R. H., Lowe, D. R., Menges, C. M., Mora, S., Pazzaglia, F. J., Sasowsky, I. R., Troester, J. W., and Wells, S. G., 1987, Central America and the Caribbean, *in* Graf, W. L., ed., Geomorphic systems of North America: Boulder, Colorado, Geological Society of America, Centennial Special Volume 2, p. 343–402.

Haxby, W. F., Turcotte, D. L., and Bird, J. M., 1976, Thermal and mechanical evolution of the Michigan Basin: Tectonophysics, v. 36, p. 57–75.

Heil, D. J., and Silver, E. A., 1987, Forearc uplift south of Panama: A result of transform ridge subduction: Geological Society of America Abstracts with Programs, v. 19, p. 698.

Hey, R., 1977, Tectonic evolution of the Cocos-Nazca spreading center: Geological Society of America Bulletin, v. 88, p. 1404–1420.

Hsü, J. T., Wehmiller, J. F., and Boutin, B., 1986, Correlation of late Pleistocene Peruvian coastal marine terraces, 14.5 to 15.5 S. latitude, by amino acid enantiometric ratio: Geological Society of America Abstracts with Programs, v. 18, p. 641.

Jordan, T. E., Isacks, B. I., Allmendinger, R. W., Brewer, J. A., Ramos, V. A., and Ando, C. J., 1983, Andean tectonics related to the geometry of the Nazca plate: Geological Society of America Bulletin, v. 94, p. 341–361.

Kelleher, M., and McCann, W., 1976, Buoyant zones, great earthquakes, and unstable boundaries of subduction: Journal of Geophysical Research, v. 81, p. 4885–4896.

Kriz, S. J., 1990, Tectonic evolution and origin of the Gulfo Dulce gold placers in southern Costa Rica: Revista Geológica de América Central, v. 11, p. 27–40.

Lew, L. R., 1983, The geology of the Osa Peninsula, Costa Rica: Observations and speculations about the evolution of part of the outer arc of the southern Central American orogen [M.S. thesis]: University Park, Pennsylvania, Pennsylvania State University, 128 p.

Lonsdale, P., and Klitgord, K. D., 1978, Structure and tectonic history of the eastern Panama Basin: Geological Society of America Bulletin, v. 89, p. 981–999.

Lundburg, N., 1982, Evolution of the slope landward of the Middle America Trench, Nicoya Peninsula, Costa Rica, *in* Leggett, J. K., ed., Trench-forearc geology: Sedimentation and tectonics on modern and ancient active plate margins: London, England, Geological Society of London, p. 131–147.

——1983, Development of fore-arcs of intra-oceanic subduction zones: Tectonics, v. 2, p. 51–61.

Madrigal, R., 1977, Terrazas marinas y tectonismo en Península de Osa, Costa Rica: Revista Geográfica, v. 86–87, p. 161–166.

Manual de Geología de Costa Rica, 1984, Volume I: Estratigrafía, Sprechmann, P., ed., San José, Costa Rica, Universidad de Costa Rica, 320 p.

Matumoto, T. G., Masakazu, O., Latham, G., and Umana, J., 1977, Crustal structure in southern Central America: Seismological Society of America Bulletin, v. 67, p. 121–134.

McGeary, S., Nur, A., and Ben-Avraham, Z., 1985, Spatial gaps in arc volcanism: The effects of collision on subduction of oceanic plateaus: Tectonophysics, v. 119, p. 195–221.

McKee, W. H., 1985, Tertiary Foraminifera of Puntarenas Province, Costa Rica [M.S. thesis]: Baton Rouge, Louisiana, Louisiana State University, 157 p.

McNutt, M. K., and Parker, R. L., 1978, Isostatic compensation in Australia: Science, v. 199, p. 773–775.

Minster, J. B., and Jordan, T., 1978, Present day plate motions: Journal of Geophysical Research, v. 83, p. 5331–5354.

Molnar, P., and Atwater, T., 1978, Interarc spreading and Cordilleran tectonics related to the age of the subducted oceanic lithosphere: Earth and Planetary Science Letters, v. 41, p. 827–857.

Montero, W., 1986, Periodos de recurrencia y tipos de secuencias sísmicas de los temblores interplaca e intraplaca en la región de Costa Rica: Revista Geológica de América Central, v. 5, p. 35–72.

Moretti, I., and Ngokwey, K., 1985, Aseismic ridge subduction and vertical motion of the overriding plate: Geodynamique des Caraibes, Symposium, Paris, France, p. 245–254.

Okaya, D. A., and Ben-Avraham, Z., 1987, Structure of the continental margin of southwestern Panama: Geological Society of America Bulletin, v. 99, p. 792–802.

Pinter, N., 1988, Isostasy and eustasy on the Osa Península, Costa Rica: Unraveling of late Quaternary geologic history through uplift and sea level change [M.S. thesis]: University Park, Pennsylvania, Pennsylvania State University, 144 p.

Pinter, N., and Gardner, T. W., 1989, Construction of a polynomial model of sea level: Estimating paleo–sea level continuously through time: Geology, v. 17, p. 295–298.

Pinter, N., Gardner, T. W., Slingerland, R., Wells, S. G., and Bullard, T. F., 1987, Late Quaternary uplift rates, Osa Península, Costa Rica: Geological Society of America Abstracts with Programs, v. 19, p. 806.

Ralph, E. K., and Michael, H. N., 1974, Twenty-five years of radiocarbon dating: American Scientist, v. 62, p. 553–560.

Shipley, T. H., and Moore, G. F., 1986, Sediment accretion, subduction, and dewatering at the base of the trench slope off Costa Rica: A seismic reflection view of the decollement: Journal of Geophysical Research, v. 91, p. 2019–2028.

Stockmal, G. S., 1983, Modeling of large scale accretionary wedge deformation: Journal of Geophysical Research, v. 88, p. 8271–8287.

Stoiber, R. E., and Carr, M. J., 1973, Quaternary volcanic and tectonic segmentation of Central America: Bulletin Volcanologique, v. 37, p. 304–325.

Taylor, F. W., Isacks, B. L., Jouannic, C., Bloom, A. L., and Dubois, J., 1980, Coseismic and Quaternary vertical movements, Sato and Malikula Islands, New Hebrides island arc: Journal of Geophysical Research, v. 85, p. 5367–5381.

Tournon, J., 1984, Magmatismes du Mesozoique a l'actuel en Amerique Centrale: l'example de Costa Rica, des ophiolites aux andesites: Memoires des Sciences de la Terre, Academie de Paris, Universite Pierre et Marie Curie, p. 84–89.

van Andel, T. G., Heath, G. R., Malfait, B. T., Heinrichs, D. G., and Ewing, J. I., 1971, Tectonics of the Panama Basin, eastern equatorial Pacific: Geological Society of America Bulletin, v. 82, p. 1489–1508.

Verdonck, D., 1990, Subduction of the Cocos Ridge and vertical movement of western Costa Rica [M.S. thesis]: University Park, Pennsylvania, Pennsylvania State University, 52 p.

Verdonck, D., and Furlong, K. P., 1988, Application of critical Coulomb wedge theory to the Pacific coast of Costa Rica: Eos, v. 69, p. 1406.

Vogt, P. R., Lowrie, A., Bracey, D. R., and Hey, R. N., 1976, Subduction of aseismic oceanic ridges: Effects of shape, seismicity and other characteristics of consuming plate boundaries: Geological Society of America Special Paper 172, 59 p.

Walcott, R. I., 1970, Flexural rigidity, thickness, and viscosity of the lithosphere: Journal of Geophysical Research, v. 75, p. 3941–3954.

Wang, C. Y., and Shi, Y. L., 1984, On the thermal structure of subduction complexes: A preliminary study: Journal of Geophysical Research, v. 89, p. 7709–7718.

Wells, S. G., Bullard, T. F., Menges, C. M., Drake, P. G., Karas, P. A., Kelson, K. I., Ritter, J. B., and Wesling, J. R., 1988, Regional variations in tectonic geomorphology along a segmented convergent plate boundary, Pacific coast of Costa Rica: Geomorphology, v. 1, p. 239–265.

MANUSCRIPT RECEIVED BY THE SOCIETY APRIL 23, 1990
REVISED MANUSCRIPT RECEIVED JUNE 17, 1991
MANUSCRIPT ACCEPTED JULY 1, 1991